

Article

Optimization of Adsorption Conditions Using Response Surface Methodology for Tetracycline Removal by MnFe₂O₄/Multi-Wall Carbon Nanotubes

Weigao Zhao ¹, Chenjie Hao ¹, Yiping Guo ², Wanfei Shao ², Yimei Tian ¹ and Peng Zhao ^{1,*} 

¹ Department of Environmental Engineering, School of Environmental Science and Engineering, Tianjin University, Tianjin 300072, China; zhaoweigao@tju.edu.cn (W.Z.); haochenjie123@tju.edu.cn (C.H.); ymtian_2000@126.com (Y.T.)

² School of Environmental and Municipal Engineering, North China University of Water Resources and Electric Power, Zhengzhou 450046, China; guoyiping@ncwu.edu.cn (Y.G.); shaowanfei@stu.ncwu.edu.cn (W.S.)

* Correspondence: zhpeng@tju.edu.cn

Abstract: In this study, the optimal conditions and effects of external factors on tetracycline adsorption by magnetic multi-walled carbon nanotubes (MMWCNTs) were established by a response surface methodology for the first time. Batch adsorption experiments showed that increasing the dosage and contact time effectively promoted the adsorption of tetracycline and maximum removal of 97.93–99.13% was achieved at pH 3–7. The pseudo-second-order model and Fourier-transform infrared spectroscopy spectra indicated that the mechanism of adsorption may be π - π electron interaction and cation- π electron bonding. Design Expert was utilized to develop a response surface methodology for the analysis and optimization of tetracycline adsorption by magnetic multi-walled carbon nanotubes. The Box–Behnken design (BBD) results showed that the optimization exhibited high significance and reliability. The main effect plots and Pareto chart indicated that pH exerted a significant individual effect on the regulation of adsorption, while 3D response surface plots and interaction effect plots exhibited a significant antagonistic interaction between pH and contact time. A maximum tetracycline removal of 99.16% was achieved under the optimal conditions of 12 mg adsorbent dosage at pH 5.43, with an adsorption time of 120 min. Mathematical and experimental results confirmed the accuracy of the established optimal conditions.

Keywords: magnetic carbon nanotubes; tetracycline; adsorption; Box–Behnken design; process optimization



Citation: Zhao, W.; Hao, C.; Guo, Y.; Shao, W.; Tian, Y.; Zhao, P. Optimization of Adsorption Conditions Using Response Surface Methodology for Tetracycline Removal by MnFe₂O₄/Multi-Wall Carbon Nanotubes. *Water* **2023**, *15*, 2392. <https://doi.org/10.3390/w15132392>

Academic Editor: Margaritis Kostoglou

Received: 17 May 2023
Revised: 20 June 2023
Accepted: 21 June 2023
Published: 28 June 2023



Copyright: © 2023 by the authors. Licensee MDPI, Basel, Switzerland. This article is an open access article distributed under the terms and conditions of the Creative Commons Attribution (CC BY) license (<https://creativecommons.org/licenses/by/4.0/>).

1. Introduction

Tetracycline (TC) is an emerging contaminant and one of the most commonly occurring antibiotics, which has been extensively utilized for medical applications due to its highly lethal effect on a variety of bacteria [1,2]. TC is difficult to degrade in organisms and can even be converted into more toxic substances [2,3]. Studies have shown that 70–90% of TC was excreted by humans and animals in an unmetabolized form, resulting in the occurrence of TC in various aquatic environments [4–7]. TC has been detected in the wastewater generated from a variety of sources including human municipal, animal husbandry, agriculture, medical, pharmaceutical, and sewage plant drainage [8–13]. TC remained in aquatic environments and has been shown to destroy microbial communities in receiving water bodies [14]. TC would induce the formation of multi-resistant genes in microorganisms, resulting in resistance to TC drugs and increasing public health risks [15–17].

In the field of organic micropollutant treatment, the adsorption process has been certified by the U.S. Environmental Protection Agency as the most efficient treatment technology and is currently the more widely used technology. [18–23]. The researchers proposed that adsorption by magnetic multi-walled carbon nanotubes (MMWCNTs) was a

highly practical process due to the simplicity of design, excellent contaminant adsorption performance, and low environmental impact [24–28]. Previous studies have indicated that the adsorption process by MMWCNTs was capable of highly efficient removal of antibiotics [29–31]. Although MMWCNTs could effectively remove TC, the optimization of the adsorption effect of MMWCNTs on TC and the interaction of various factors on treatment efficiency have not been documented [32,33].

According to the survey, the conditional optimization methods used in the adsorption process are listed in Table S1 [32,34–44]. Among the experimental methods, response surface methodology (RSM) was utilized to fit a mathematical model and experimental data, to analyze the relationship between influencing factors and response values, and to obtain the optimal operating conditions for a specific system [25,38,41,45–48]. In RSM, both Box–Behnken design (BBD) and central composite design (CCD) are plane-centered design methods. Compared with CCD, BBD is more inclined to solve the local optimal solution (the level of BBD factors is generally less than 5) [20,49,50]. As one of the most commonly used response surface methods, the BBD avoided extreme conditions, and it had a moderate number of experiments, simple and efficient software operation, and high reliability and accuracy of optimization results, without massive training data for the simulation [25,29,51–53]. The removal rate of TC in this study was affected by three factors (pH, time, and adsorbent dosage). Apparently, BBD is more suitable for this study. In this paper, the studies on the optimization of TC removal and multiwall carbon nanotube (MWCNTs) adsorption process by RSM-BBD were summarized, which were recorded in Tables S2 and S3. Table S2 [54–57] and Table S3 [58–66] showed that BBD could improve adsorption efficiency and save resources in the fields of MWCNTs adsorbent and TC removal, respectively [54,58]. At present, RSM-BBD optimization of MMWCNTs adsorption TC needs further practice.

In this study, MMWCNTs were successfully synthesized using a previously reported method for TC removal. To our knowledge, no one has ever used RSM-BBD to simulate, analyze and optimize the process of TC adsorption on MMWCNTs, using three independent variables: adsorbent dosage, pH, and time. The independent variable input values and the individual effects of the three factors were studied using batch adsorption experiments. The adsorption mechanism was established according to adsorption kinetics fitting and characterization results. Analysis of variance (ANOVA) was used to examine the significance of the model. The interactive effects of factors were assessed using response surface plots, interaction effect plots, and Pareto chart analysis, allowing the related parameters affecting removal efficiency to be statistically optimized. This study provides a feasible method for optimizing and adjusting TC adsorption conditions while enhancing the potential for the practical application of magnetic carbon nanotubes. The optimization of external conditions promotes the quality and efficiency of the TC adsorption process, providing a reference method for the improvement of TC removal efficiency. The process optimization method of TC adsorption by MMWCNTs should further adapt the actual operating conditions to increase the optimization parameters and pollutant types.

2. Materials and Methods

2.1. Reagents and Instruments

The multi-walled carbon nanotubes (tubes diameter of 8–10 nm) employed to prepare the adsorbent material were purchased from Helue Lida Power Materials Co., Ltd. (Xinxiang, China). Analytically pure NaOH, ferric chloride, and manganese chloride were supplied by Yingda Rare Chemical Reagents Factory Co., Ltd., (Tianjin, China). TC (98% purity) was supplied by Hefei Bomei Biological Technology Co., Ltd. (Hefei, China). Nitric acid, sodium hydroxide, and anhydrous ethanol (Shuangshuang Chemical Co., Ltd., Laiyang, China) were of analytical grade.

An electronic balance (BSA124S-CW, Sartorius AG, Mettler Toledo Instrument Co., Ltd., Shanghai, China) was used to weigh materials and a pH meter (PB-10, Sartorius AG) was used to determine the pH of solutions. A digital display electric constant temperature

water bath (XMTD-204, Honour Instrument Shaker Co., Ltd., Tianjin, China) was used to heat carbon nanotube solutions and the iron–manganese mixture. A JJ-1 electric mixer and GL-88-b type vortex mixer (Haimen Kyling-bell Lab Instruments Co., Ltd., Haimen, China) was used for solution mixing.

2.2. Experimental Methods

2.2.1. Preparation of MMWCNTs Composites

The MMWCNTs (Size is about 10–50 nm) were prepared using a co-precipitation method previously reported by Zhao et al. [7]. The specific preparation methods of MMWCNTs, as well as Transmission Electron Microscope (Figure S1a,b), zeta potential (Figure S1c), and Fourier-transform infrared spectroscopy (Figure S1d) scanning electron microscope (Figure S1e) and Energy Dispersive X-ray spectroscopy (Figure S1f) characterization, are all provided in the Supplementary Materials.

2.2.2. Batch Adsorption Experiments

In this study, the dosage of adsorbent, pH, and the adsorption time were assessed as the variable factors for batch adsorption experiments. According to previously reported studies, adsorbent dosage directly affects the number of adsorption sites and the mass transfer efficiency [25,67]. Due to protonation and deprotonation, the surface charge of the material and the chemical forms of organic compounds are transformed under varying pH conditions, affecting electrostatic and chemical bonding between TC and adsorbents [8,67–70]. The influence of contact time on adsorption is indicative of the adsorption reaction kinetics and can be used to establish the adsorption mechanism [4,17,70].

For the adsorption time batch experiment, 50 mL of the 20 mg/L TC solution was placed in a 150 mL conical flask, then 12 mg of MMWCNTs were accurately weighed using an electronic balance and mixed with the TC solution. The pH of the solution was maintained at 7 by adding 1 M nitric acid or sodium hydroxide in a dropwise manner as required. The conical flask was fixed in a thermostatic water bath at a temperature of 298.15 K, with continual oscillation at 140 rpm for 1500 min. Samples were collected from a conical flask for measurements at specified time points (1, 2, 5, 8, 10, 15, 20, 25, 30, 45, 60, 90, 120, 720, 840, 960, and 1440 min). For batch experiments assessing the effects of varying pH, the maximum adsorption time was fixed at 1440 min, with the pH of the solution varying from pH 2–10, while for adsorbent dosage batch experiments, the dosage varied from 5 to 13 mg, with all other conditions remaining constant as described above. After adsorption, the adsorbent and TC solution mixture were left to stand for 30 min before 5 mL of supernatant was taken from the conical flask with a gel head dropper and filtered through a 0.45 µm cellulose filter membrane. The absorbance of the filtered sample was measured using a spectrophotometer (TC adsorption wavelength of 360 nm). The experiments were repeated in triplicate under the same conditions, with the average values used for further analysis. The solution removal rate (%) and equilibrium adsorption capacity q_e (mg/g) were calculated according to Equation (1) and Equation (2), respectively.

$$\text{Removal rate} = (C_0 - C_e) / C_0 \times 100\% \quad (1)$$

$$q_e = (C_0 - C_e) / m \times V \quad (2)$$

Here, C_0 represents the initial concentration of TC before adsorption (mg/L); C_e represents the concentration of TC after adsorption (mg/L); m indicates the mass of MMWCNTs (mg); and V indicates the volume of the solution.

2.3. Box–Behnken Design Model

According to the TC removal efficiency under different conditions, the range of conditions associated with higher removal rates was preliminarily determined [51]. As shown in Table S4, adsorbent dosage (A), adsorption time (B), and solution pH (C) values were

divided into three levels (−1, 0, 1), with adsorbent dosage levels of 6, 9, and 12 mg, adsorption time levels of 120, 300, and 480 min, and pH value levels of 4, 5, and 6. In total, 17 experiments were simulated using Design Expert (v. 10.0.3) software, with TC removal efficiency set as the response (Y) for each respective variable. ANOVA and residual values were used to establish the fitness of the model, the rationality of equations, and the significance of the response [52,71]. The main effect plots and Pareto chart for different factors were analyzed to assess the individual effect of each factor, with the interactions between factors then established using 3D response surface plots, Pareto chart, and interaction effect plots [26]. The RSM was employed to identify the exact external condition values capable of achieving maximum removal efficiencies [72]. Actual measurement values verified the predicted effect of the model.

The nonlinear quadratic model adopted for response surface analysis is shown in the Supplementary Materials.

3. Results and Discussion

3.1. Batch Adsorption Experiments

3.1.1. Effect of Dosage

With the initial increase in dosage of MMWCNTs from 5 mg to 7 mg the removal rate increased linearly from 78% to 87% due to the increase in active sites and the high available concentration of TC (Figure 1). However, due to the agglomeration of adsorbents, further increases in adsorbent dosage led to a decline in the total adsorbent surface area and the availability of active surface sites [73]. Increasing adsorbent dosages from 8 to 12 mg resulted in a smaller increase in the adsorption efficiency (<5%), with the adsorption rate becoming slower and gradually stabilizing from a dosage of 12 mg upwards, achieving a maximum TC removal rate of 99.5%. The relationship between the adsorption capacity and removal rate exhibited an inverse trend, with an increase in adsorbent dosage from 5 to 6 mg resulting in a reduction in adsorption capacity from 202.6 mg/g to 145 mg/g, with a further increase in dosage to 13 mg causing the adsorption capacity to reduce to 80 mg/g. With the increase in TC removal and adsorbent dosage, the adsorption mass transfer efficiency declined, due to TC molecules saturating the surface adsorption sites and reducing the total surface area of the adsorbent [74]. The final adsorption capacity was maintained at about 83 mg/g (equilibrium adsorption capacity of 20 mg/L TC). In summary, increasing adsorbent dosage can promote TC removal, although adsorption is reduced with excessive TC concentrations. According to the experimental results, at a concentration of 20 mg/L TC, 6–12 mg was selected as the adsorbent dosage input value for RSM analysis.

3.1.2. Effect of pH

As shown in Figure 2, the optimal pH range for TC removal by 12 mg MMWCNTs within 24 h was pH 3–7, achieving a removal rate of 97.59–99.31%. The q_e reached a maximum of 83 mg/g at pH 3 and gradually declined as the pH increased to pH 6 and above. At pH < 3.0 and >7.0, the adsorption effect of TC reached a maximum of 90–95%, with an adsorption capacity of <80 mg/g. Under different pH conditions, TCs showed different functional groups, making the adsorption effect of MMWCNTs on TCs inconsistent. In aqueous solutions, TC exhibits three pK_a values of 3.3, 7.7, and 9.7 [5,75], due to its characteristics of containing electron-deficient amino and enone groups, as well as an electron-rich phenol ring [67,69]. At pH < 3.3, the solution is acidic, resulting in the dimethylamine group attracting protons and TCH_3^+ being the dominant component in the TC group, causing the TC molecules in the solution to exhibit cationic properties [17,76], with the potential of MMWCNTs being approximately 32 mV (Figure S1c). Despite strong interactions that resulted in the adsorption of more than 90% of TC in solution, adsorbents and contaminants are subject to electrostatic repulsion. At $3.3 < \text{pH} < 7.7$, the dominant group in TC was TCH_2^0 , which has no external electrical properties, indicating that the adsorption of TC reached a peak level without the occurrence of electrostatic repulsion [4].

At $\text{pH} > 7.7$, TC was dominated by negatively charged TCH_2^- and TC^{2-} , while the potential of MMWCNTs was about -15mV due to the deprotonation of carboxyl groups on the adsorbent [10,15,77–79]. At pH_{pzc} , adsorption could not be attributed to electrostatic interactions, and therefore, the removal of TC by MMWCNTs was higher at $\text{pH} 3\text{--}7$. The reason may be that the pH is in the range of $3\text{--}7$, the TC amphiphilic form (TCH_2^0) exists, the TC molecules have almost no electrostatic attraction or repulsion to MMWCNTs, and the effect of pH on TC adsorption is negligible. Whereas, when the pH is less than 3 or more than 7, TC and MMWCNTs have the same charge, and a certain degree of electrostatic repulsion is generated, which is not favorable for the adsorption of TC by MMWCNTs. Based on the above analysis, the pH input value was set to $4\text{--}6$ in the RSM.

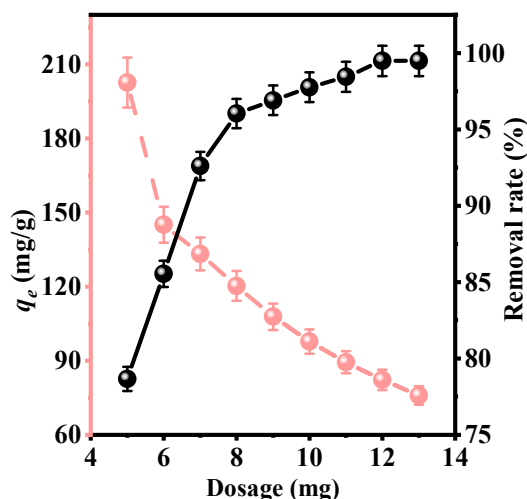


Figure 1. Effect of adsorbent dosage on the Tetracycline (TC) removal rate and adsorption capacity of magnetic multi-walled carbon nanotubes (MMWCNTs). Reaction conditions included an initial TC concentration of 20 mg/L , $\text{pH} 7.0 \pm 0.1$, contact time of 1440 min , and reaction temperature of 298.15 K . (The black data points in the graph represent the removal rate and the red data points represent the q_e).

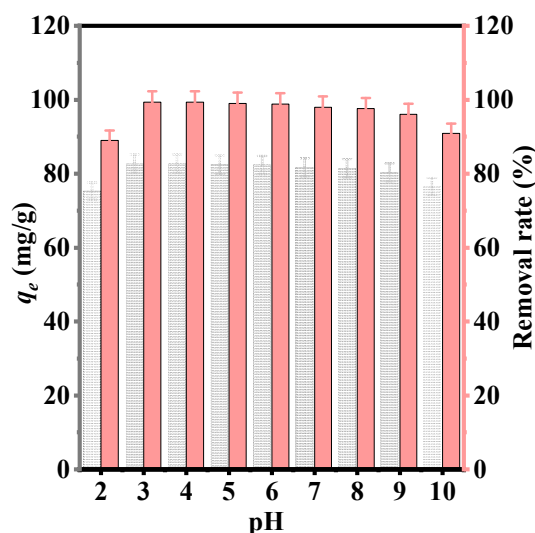


Figure 2. Effect of pH on the TC removal rate and adsorption capacity of MMWCNTs. Reaction conditions included an initial TC concentration of 20 mg/L , adsorbent dosage of 12 mg , contact time of 1440 min , and reaction temperature of 298.15 K . (The red data points in the graph represent the removal rate and the black data points represent the q_e).

3.1.3. Effect of Time

The TC adsorption capacity of MMWCNTs increased to 82.33 mg/g, within 720 min (Figure S2). The q_e of TC by MMWCNTs reached 80 mg/g prior to 200 min and remained around 83 mg/g for the remainder of the contact time, reaching adsorption equilibrium after 700 min. Within the initial 50 min of the reaction, the high concentration of TC in the solution enhanced the effect of mass transfer, with the adequate availability of adsorption sites providing a high probability of collision between molecules, resulting in a rapid TC adsorption rate [9,12]. After MMWCNTs had rapidly adsorbed a huge amount of TC at 150 min, many of the adsorption sites were occupied and the adsorption rate declined. Therefore, based on these findings the contact time range input value for RSM analysis was 120–480 min.

3.1.4. Adsorption Kinetics

Figure 3 presents the results of data fitting using the pseudo-first-order, pseudo-second-order, Elovich, Weber and Morris, and Banham models. The equations applied for the different models are provided in the supporting information, with the obtained kinetic parameters shown in Table S5. The results demonstrate that the pseudo-first-order model data fitting was good, with an R^2 of 0.944, although the adsorption capacity calculated using this model was 80.57 mg/g, which differed from the experimental results. The determination coefficients of the Elovich and Bangham models were 0.729 and 0.668, with q_e values of 87.05 and 87.82 mg/g, respectively. The Weber and Morris model classified the adsorption process as being surface adsorption and slow intra-particle diffusion. However, the R^2 using the Weber and Morris model was 0.412 and the straight line failed to pass through the origin of the coordinates. The pseudo-second-order kinetic model successfully explained the experimental data ($R^2 = 0.975$ and $q_e = 84.13$ mg/g), indicating that the adsorption of TC by MMWCNTs may occur via chemical adsorption, due to the sharing or interchange of electrons between adsorbents and adsorbates resulting in valence forces. The chemical adsorption process can be separated into two phases, with (1) TC initially adsorbed on the surface forming a monolayer and (2) chemisorption mechanisms dominating once monolayer physical adsorption approaches saturation [17,80,81]. In summary, pseudo-second-order kinetics were optimal for depicting the TC adsorption process on MMWCNTs.

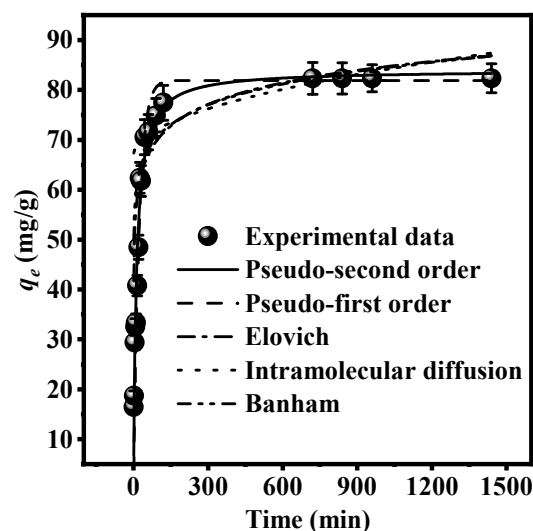


Figure 3. Experimental data of adsorption kinetic and nonlinear fitting of the pseudo-first-order, pseudo-second-order, Elovich, Weber and Morris, and Banham models for TC adsorption. Reaction conditions included an initial TC concentration of 20 mg/L, adsorbent dosage of 12 mg, pH 7.0 ± 0.1 , and reaction temperature of 298.15 K.

3.1.5. Mechanism of TC Adsorption by MMWCNTs

According to the results of FT-IR infrared spectroscopy, single-factor experiments with pH variation and adsorption kinetics results, the proposed TC adsorption mechanism (Figure S3) can be explained by the following two mechanisms: (1) π - π interactions between TC's polarity/ionization groups (including amino, carboxyl, phenol, ethanol, and acetone) (Figure S4) and oxygen-containing functional groups on MMWCNTs, (carboxyl and hydroxyl groups) (Figure S1d), with some groups serving as π -electron donors (hydroxyl) or π -electron receptors (carboxyl, conjugated enone structures) [69,82], while the TC ring structure and hexagonal cells in MMWCNTs form π - π stacked interactions [70,75,83,84]. (2) The formation of cation- π bonds due to electrostatic forces between cation-induced polarized regions and the quadrupole of π -electron-rich aromatic structures [85]. TC is amphoteric in a pH range of 3–7, with a cationic dimethyl amino group ($pK_a = 9.7$), resulting in π electrons on MMWCNTs easily forming cation- π bonds. The amino and hydroxyl groups on TC molecules tend to form strong hydrogen bonds with carbon-based adsorbents [68].

3.2. Box-Behnken Design Model

3.2.1. Modeling and Statistical Analysis

Table 1 demonstrates the experimental design, experimental results, and the model-predicted TC removal rate (%). The experimental results show that TC removal ranged from 73.35% to 97.88%, with an overall deviation of <3%. Kinetic analysis (Table S6) shows the results of data fitting using four models (Linear, 2FI, Quadratic, Cubic), with F-test analysis indicating that the quadratic model exhibited the highest level of significance (F-value (Fisher rate) = 22.10; p -value (prob > F) = 0.0002; F-value of the lack of fit = 0.34), indicating that most of the variation could be explained by the quadratic model regression equation [38,86]. The influence of noise probability was only 0.02% with a signal-to-noise ratio of >4, while the p -value of lack of fit was 0.798, indicating that misfit error could be ignored. The calculation methods are described in detail in the Supplementary Materials. Equation (3) describes the quadratic model equation for the TC removal rate with varying dosage, contact time, and pH, with negative interaction terms (AB, BC, AC, B^2 , C^2) indicating an antagonistic effect on the removal rate [25]. All the analyses presented in this paper were based on quadratic model analysis.

$$Y = 91.28 + 1.66 \times A + 1.54 \times B + 0.2 \times C - 4.17 \times A \times B - 3.08 \times A \times C - 10.4 \times B \times C - 0.32 \times A^2 + 2.29 \times B^2 - 8.74 \times C^2 \quad (3)$$

where Y represents the TC removal rate by MMWCNTs; A represents the adsorbent dosage; B represents the adsorption time; C represents the pH value.

Table 1. Experimental factor level values with experimental and predicted TC removal values at each factor level.

Run Order	Dosage (mg)	Time (min)	pH	TC Removal (%)	
				Experimental	Predicted
1	9	300	5	89.56	91.28
2	9	300	5	94.55	91.28
3	9	300	5	90.32	91.28
4	12	300	6	82.29	81.01
5	6	480	5	97.88	97.31
6	12	480	5	91.65	92.28
7	9	300	5	88.65	91.28
8	9	480	4	97.28	96.57
9	9	120	6	93.19	93.90
10	6	120	5	86.52	85.89
11	9	300	5	93.34	91.28
12	6	300	6	83.93	83.85

Table 1. Cont.

Run Order	Dosage (mg)	Time (min)	pH	TC Removal (%)	
				Experimental	Predicted
13	9	480	6	75.54	76.19
14	12	120	5	96.97	97.54
15	9	120	4	73.35	72.70
16	6	300	4	76.01	77.29
17	12	300	4	86.68	86.76

3.2.2. Analysis of Variance

ANOVA was performed to verify the statistical significance of the experimental design and establish the interactions between independent variables and response effects (Table S7) [41,72]. ANOVA subdivides the total variation into two components, with variation associated with either the model or experimental error [87,88]. F- and *p*-values (prob > F, confidence interval = 95%) for the model were obtained as shown in Table S7. The F-value of the lack of fit (0.34) and the *p*-value (>0.05) were insignificant, proving that the second-order model with interactive effects was adequate for approximating the RSM [89]. *p* (AB) = 0.006, *p* (BC) = 0 and *p* (C²) = 0 were more significant than the other interaction terms, while the *p*-values of B (0.796) and B² (0.768) were appreciably greater than 0.05, indicating that the influence of these factors on the response value could be ignored. The accuracy of the predictions generated by the model was verified according to the R² (0.9660), R_{adj}² (0.9223), and standard deviation (2.15). A total of 7.7% of the total variation could not be explained exclusively by the model [46,53]. Overall, the ANOVA indicated that the BBD model exhibited excellent accuracy and reliability for TC adsorption by MMWCNTs [52].

3.2.3. Main Effect of Variables

The main effect of variables represents the regulatory effect of a specific individual factor on the response value [25]. The main effect plot for varying dosage (Figure S6a) demonstrated that an increase in adsorbent dosage from 6 to 12 mg resulted in an increase in the average removal rate from 86.08% to 89.39%, while the curve slope decreased with increasing dosage from 0.778 (6–9 mg) to 0.325 (9–12 mg), indicating that the promotive effect of dosage on the removal rate decreased with increasing dosage levels. Initial increases in adsorbent dosage increase the surface area available for TC adsorption. However, at an adsorbent dosage of 13 mg, the *q_e* of the adsorbent was close to the equilibrium adsorption capacity of 83 mg/g, leading to a decrease in the main effect of this factor. According to the results of variance analysis, the *p*-values of A and A² were 0.082 and 0.065, respectively. Pareto chart analysis showed that the contributions of A and A² to the removal rate were 0.41% and 0.39%, respectively, indicating that the effect of dosage on the removal of TC was weak.

The main effect plot for pH (Figure S6b) indicated that the TC removal rate increased rapidly from 83.33% (pH 4) to 92.16% (pH 5), then decreased to 83.73% (pH 6), with the slope of the curve altering by 200%, while the intersection angle between the curve and reference line was the largest compared with the other two factors. Variance analysis showed a *p*-value for pH of 0.066 (<0.05) and a *p*-value for pH² of 0, indicating a strong individual effect. According to Figure S1c, the pH_{pzc} of MMWCNTs was 4–5, with TCH₂⁰ being the dominant species at pH 5, indicating that adsorption was far greater than electrostatic repulsion. Once the pH value deviates from pH_{pzc}, a small portion of TCH[−] groups on TC molecules will repel the adsorbent surface. Therefore, compared with contact time and dosage, the pH value exhibited the most significant individual effect on the rate of TC removal by MMWCNTs.

The main effect plot for adsorption time (Figure S6c) was drawn from the average TC removal rate values at 120, 300, and 480 min in 17 groups of experiments, according to

the RSM. Before the 300 min, the curve slope was 0.0014, running almost parallel to the reference line, with the removal rate changing by 0.25%. After 480 min, the average TC removal rate increased to 90.58%. Variance analysis demonstrated that contact time exerted a low effect on TC removal (p -value for time = 0.796, p -value for time² = 0.768). Due to the affinity among adsorbates and adsorbents and the excessive concentration of TC, the high mass transfer efficiency resulted in the adsorption equilibrium being reached within a short time and the adsorption time indicating a weak individual effect on the removal rate.

The standardized Pareto chart (Figure 4) indicated the influence of the items in Equation (3) on TC removal [26,90]. The results showed that the most significant factors affecting TC adsorption by MMWCNTs were pH² (standardization effect = 8.27%) and pH-time (standardization effect = 10.13%) interactions, indicating an acceptable level of agreement with the observed results shown in Table S7 (p -value for pH² and pH-time = 0). These results validate the previously established conclusion, that the individual effect of pH was the most significant (pH (4.53%), pH² (8.27%), pH-time (10.13%), and pH-dosage (4.06%).

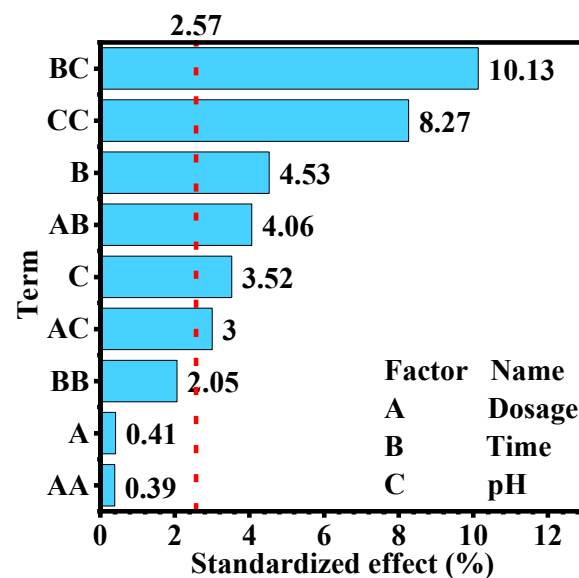


Figure 4. Pareto chart of the interactive effect of experimental factors (dosage, time and pH) with TC removal as the corresponding variable ($\alpha = 0.05$).

3.2.4. Interaction of Contact Time and Adsorbent Dosage

To understand the interactions of various factors on removal, contour plots, 3D response surface plots, and interaction effect plots were constructed according to the proposed regression model (Equation (2)) [91]. Figure 5a,b show contour plots and response surface plots for adsorption time and adsorbent dosage. As the adsorbent dosage increased from 6 to 12 mg and the contact time was extended from 120 to 480 min, the TC removal rate gradually increased. TC removal reached a maximum of 97% in 480 min at an adsorbent dosage of 6 mg and 120 min at an adsorbent dosage of 12 mg. The lowest adsorption efficiency (86%) occurred at a dosage of 6 mg and a contact time of 120 min, with the extension of adsorption time increasing the collision probability for TC molecules and the adsorbent, while the rise in adsorbent dosage increases the accessibility of the exchangeable surface adsorption sites. When a maximum contact time and dosage were applied (480 min contact time and 12 mg dosage), the adsorption efficiency decreased (92%) due to the antagonistic effect of time and dosage. Figure S7 shows an interaction effect plot for time and dosage, which was utilized to describe the dynamic interaction between various factors. From 120 to 300 min, the curves intersected, and the slope varied from 0.036 at 6 mg, and -0.044 at 9 mg, to 0.069 at 12 mg, indicating a distinct interaction between the time and dosage. In the Pareto chart (Figure 4), the interactive contribution of time and dosage on the removal rate was 4.06% > 2.57% (minimum statistically significant effect magnitude), indicating the

significance of time–dosage interactions. In summary, the interactive effect of adsorbent dosage and contact time on TC removal was significant and substantial (p -value = 0.006, Table S7).

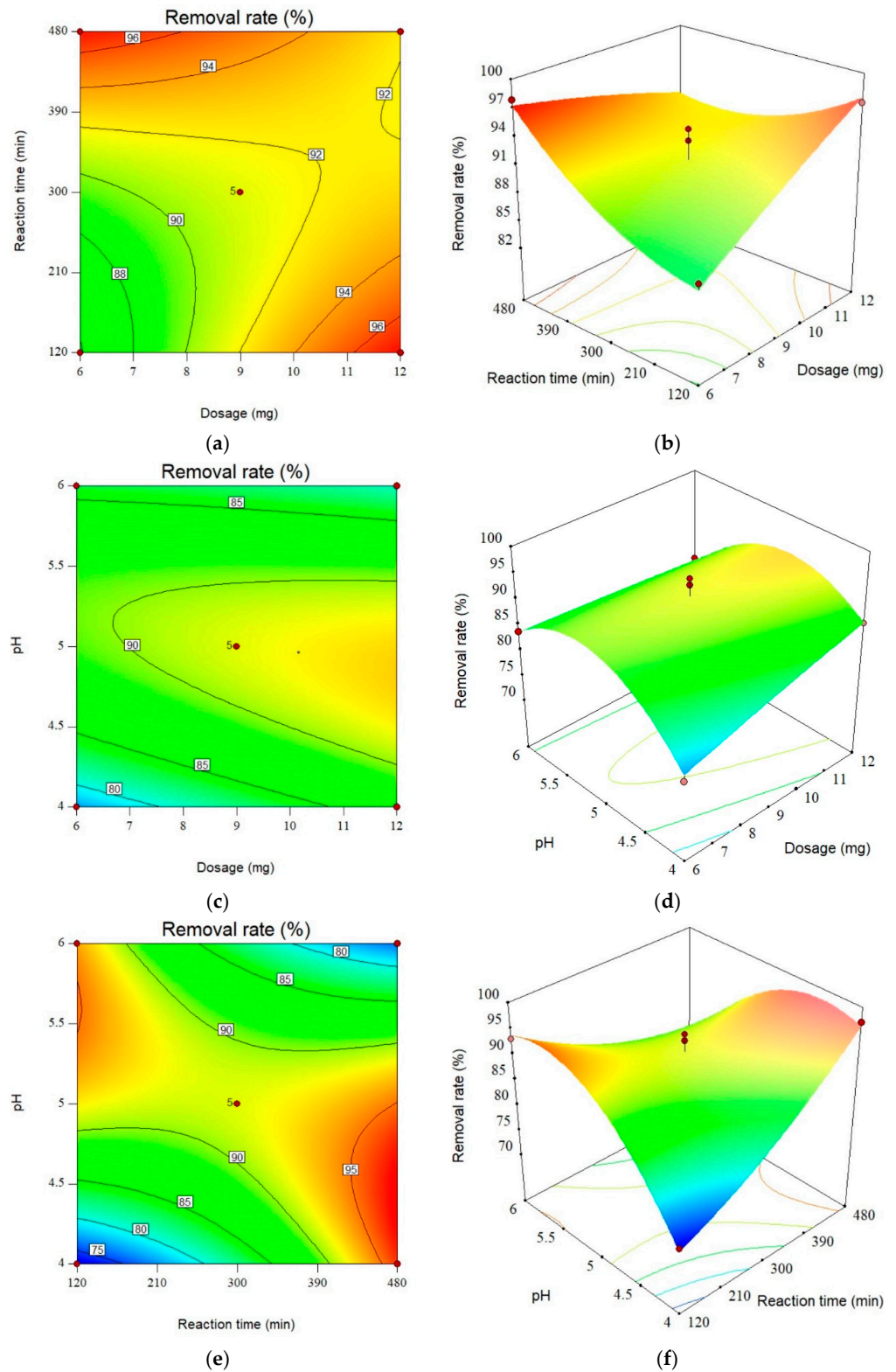


Figure 5. Interaction of dosage, time, and pH on TC removal efficiency: (a) Contour plot of time and dosage (pH 5); (b) Response surface plot of time and dosage (pH 5); (c) Contour plot of pH and dosage

(contact time = 300 min); (d) Response surface plot of pH and dosage (contact time = 300 min); (e) Contour plot of pH and time (dosage of 9 mg); (f) Response surface plot of pH and time (dosage of 9 mg). (The color changes from blue to red, indicating that the removal rate is getting higher and higher).

3.2.5. Interaction of Adsorbent Dosage and pH

Figure 5c,d are contour and 3D response surface plots for pH and adsorbent dosage. The results show that the removal rate initially increased and then decreased with the rise in pH from 4 to 6. TC removal occurred monotonically (86–93%) with increasing dosage from 6 to 12 mg. The peak TC removal rate (92%) occurred at pH 5 and a dosage of 12 mg, which was attributed to the π - π electron interactions and cationic- π electron bonds between MMWCNTs and TC molecules at pH_{pzc} (with weak electrostatic repulsion). The results indicate that increasing dosage does not affect the relationship between pH and the TC removal rate, and neither does increasing pH affect the relationship between dosage and the TC removal rate, verifying the insignificance of pH and adsorbent dosage interactions. As shown by the pH and adsorbent dosage interaction plot (Figure S7), with increasing pH, TC removal initially increased to a maximum level (90–95%) and then decreased to 85%. The three interaction curves demonstrate that the variation in adsorbent dosage did not alter the overall trend, although the removal effect could be improved. At pH 5–6, the slope fluctuated from 8.27 (6 mg) to 6.919 (9 mg) to 12.02 (12 mg), indicating the low level of interaction between pH and adsorbent dosage. The same result was shown by the Pareto chart (Figure 4), where the contribution of interaction between pH and the adsorbent dose was only 3%. Therefore, the interactive effect of dosage and pH on TC removal was low (p -value = 0.024, Table S7).

3.2.6. Interaction of Contact Time and pH

Figure 5e,f display the contour plot and response surface plot for the pH and contact time of adsorption efficiency. The maximum percentage of TC removal was achieved at 480 min and pH 4.5. At pH levels < 5, a significant increase in the amount adsorbed was observed from 120 to 480 min, while the opposite trend was observed at pH levels > 5. Similarly, within 300 min, the adsorption effect increased with higher pH values (from 80% to 94%), while from 300 to 480 min, the adsorption effect decreased with increasing pH values from 4 (96%) to 6 (82%), further proving the antagonistic interaction between pH and contact time. Therefore, simultaneous increases in pH and contact time significantly reduced the TC adsorption effect. As shown by the pH and time interaction plot (Figure S7), in which from 120 to 480 min the varying pH initially increased from 4 to 6 the TC removal rate (73.35–93.19%) at a pH of 4 and then decreased the removal rate (97.28–75.54%) at a pH of 6, verifying the occurrence of antagonistic interactions. Pareto chart analysis revealed that pH-contact time contributed 10.13% to the removal rate and ANOVA (F-value = 93.62, p -value = 0) demonstrated that the interaction between pH and contact time was most significant compared with the other interaction terms.

3.3. Validation of Box–Behnken Design Optimization

To determine the practical application effect of RSM-BBD on the parameter optimization of TC adsorption by MMWCNTs, the optimum conditions for TC removal by the MMWCNTs adsorbent were investigated with varying adsorbent dosage, pH, and adsorption time [51].

Design Expert software suggested that pH 5.4, an adsorbent dosage of 12 mg, and contact time of 120 min, were the optimum conditions to achieve a maximum TC removal by MMWCNTs of 99.16%, with desirability of 0.984.

Table 2 shows the validation results for 10 groups of different experimental conditions simulated by Design Expert software (v.10.0.3). The experimental results show that the TC removal rate reached 98.86% under optimal conditions, with an error level of 0.3%. The overall error of the 10 groups of experiments was <1%, proving the accuracy of the

model prediction. Overall, RSM-BBD was found to reliably simulate TC adsorption by MMWCNTs, allowing effective method optimization.

Table 2. Experimental design conditions and the TC removal response (%) of each run. Initial TC concentration: 20 mg/L and temperature: 298.15 K.

Run Order	Parameter			Experimental (%)	Predicted (%)	Expectation	Deviation (%)
	Dosage (mg)	Time (min)	pH				
1	12.0	120	5.4	98.86	99.16	0.984	−0.300
2	12.1	120	5.5	98.12	98.99	0.981	−0.870
3	12.2	123	5.5	98.11	98.92	0.980	−0.810
4	11.8	120	5.4	98.00	98.96	0.968	−0.960
5	11.9	120	5.1	97.98	98.15	0.965	−0.170
6	12.0	136	5.5	97.98	97.87	0.959	0.110
7	12.1	480	4.2	97.96	97.32	0.948	0.640
8	12.3	479	4.3	97.83	97.27	0.947	0.560
9	11.9	479	4.2	97.06	97.32	0.945	−0.260
10	11.9	479	4.2	97.01	97.33	0.943	−0.320

4. Concluding Remarks

In this study, RSM-BBD was employed to establish a quadratic polynomial model to analyze the TC adsorption process by MMWCNTs, in terms of dosage, pH, and time. The main conclusions are as follows: (1) ANOVA established a high level of significance (F-value = 22.1, p -value < 0.05), fitness ($R^2 = 0.966$ and $R_{adj}^2 = 0.922$), and accuracy (the residual fit the normal probability distribution) of the model. (2) From the analysis of the Pareto Diagram and main effect diagram, the promoting effect of dose on removal rate decreases with the increase in dose level, and the effect on TC is weak. Main effect plots demonstrated that in the pH range from 4 to 6, the average removal curve slope changed by 200%, with the effect of pH on TC removal being the most significant (contribution of pH^2 on removal = 8.27%, F-value = 69.60, p -value = 0). (3) The pseudo-second-order model was successfully applied to explain the adsorption kinetics ($R^2 = 0.975$ and $q_e = 84.1$ mg/g). The TC adsorption mechanism involved π - π electronic interaction and cation- π electronic bonding. (4) The response surface plots, Pareto chart, and variance analysis established that the strongest antagonistic interaction occurred between contact time and pH (contribution of time-pH = 10.13%, F-value = 93.62, p -value = 0). In addition, the correlations of pH with dosage and dosage with time were not significant. (5) The maximum TC removal efficiency of 99.16% was achieved at an adsorbent dosage of 12 mg, pH 5.4, within 120 min, and desirability = 0.984. The verification experiment results indicated that the actual removal under optimal conditions was 98.86%, indicating that the RSM-BBD model could effectively be used for optimizing TC adsorption by MMWCNTs. The optimization method used in this paper determined the optimal adsorption conditions and the influence of external factors, promoting the industrial application of MMWCNTs.

Supplementary Materials: The following supporting information can be downloaded at: <https://www.mdpi.com/article/10.3390/w15132392/s1>, Figure S1: (a) Transmission electron microscopy observation of MWCNTs at 20 nm (Quanta-250, FEI, Waltham, MA, USA); (b) Transmission electron microscopy observation of MMWCNTs at 20 nm (Quanta-250, FEI, US); (c) Zeta potential of MWCNTs and MMWCNTs (pH = 2–10); (d) FT-IR of MnFe₂O₄, MWCNTs and MMWCNTs [7]; (e) Characterization of MMWCNTs by scanning electron microscope (SEM, Quanta-250, FEI, USA) [7]. (f) Characterization of MMWCNTs by Energy Dispersive X-ray spectroscopy [7]; Figure S2: Effect of adsorption time on TC adsorbent adsorption capacity. Initial TC concentration of 20 mg/L; adsorbent dosage of 12 mg; pH 7.0 ± 0.1, reaction temperature of 298.15 K; Figure S3: Schematic mechanism of the π - π interactions and cationic- π bonding between MMWCNTs and TC molecules; Figure S4: The main components of TC (phenolic hydroxyl group (C-OH); dimethyl amino group (-N(CH₃)₂); acylamino group (-CONH₂); and the keto-enol conjugated double bond system) and the acidity

coefficient of each component; Figure S5: Residual diagnostic chart of TC adsorption test results: (a) Normal % probability versus internally studentized residuals; (b) Residuals versus predicted values; (c) Residuals versus run number; (d) Plot of model predicted value versus actual experimental value; Figure S6: Main effect plots for (a) Dosage; (b) pH and (c) Reaction time for the response surface method; Figure S7: Interaction plot of dosage, reaction time and pH; Table S1: Optimization methods of various adsorption processes; Table S2: Current status of BBD-RSM in the optimization of TC adsorption process with different adsorbents; Table S3: Current status of BBD-RSM in the optimization of MWCNTs adsorption process with different adsorbents; Table S4: The experimental factors, levels and coded values for TC removal experiment, including three factors and three response levels; Table S5: Parameters of kinetic models for the adsorption of TC by MMWCNTs; Table S6: Statistical analysis of the effectiveness of models for modeling the process of TC adsorption by MnFe₂O₄/MWCNTs (confidence interval = 95%); Table S7: Analysis of variance (ANOVA) for TC removal according to the response surface quadratic model (confidence interval: 95%).

Author Contributions: W.Z.: Investigation, Methodology, Experiment, Data curation, Formal analysis, Writing—original draft preparation, Writing—review & editing. C.H.: Writing—review & editing, Data curation. Y.G.: Writing—review & editing. W.S.: Writing—review & editing, Methodology, Experiment, Data curation. Y.T.: Supervision, Validation, Writing—review & editing, Project administration. P.Z.: Supervision, Validation, Writing—review & editing. All authors have read and agreed to the published version of the manuscript.

Funding: This work was supported by the State Key Laboratory of Pollution Control and Resource Reuse (PCRRF21038 and PCRRF19018) and the Science & Technology Research and Development Plan Joint Fund in Henan Province (No. 222103810014).

Data Availability Statement: The datasets used and/or analyzed during the current study are available from the corresponding author on reasonable request.

Conflicts of Interest: The authors declare that they have no known competing financial interest or personal relationships that could have appeared to influence the work reported in this paper.

References

1. Escobar-Huerfano, F.; Gómez-Oliván, L.M.; Luja-Mondragón, M.; SanJuan-Reyes, N.; Islas-Flores, H.; Hernández-Navarro, M.D. Embryotoxic and teratogenic profile of tetracycline at environmentally relevant concentrations on *Cyprinus carpio*. *Chemosphere* **2020**, *240*, 124969. [[CrossRef](#)] [[PubMed](#)]
2. Cui, H.; Wang, J.; Feng, K.; Xing, D.F. Digestate of Fecal Sludge Enhances the Tetracycline Removal in Soil Microbial Fuel Cells. *Water* **2022**, *14*, 2752. [[CrossRef](#)]
3. Sarmah, A.K.; Meyer, M.T.; Boxall, A.B.A. A global perspective on the use, sales, exposure pathways, occurrence, fate and effects of veterinary antibiotics (VAs) in the environment. *Chemosphere* **2006**, *65*, 725–759. [[CrossRef](#)] [[PubMed](#)]
4. Jin, J.H.; Yang, Z.H.; Xiong, W.P.; Zhou, Y.Y.; Xu, R.; Zhang, Y.R.; Cao, J.; Li, X.; Zhou, C.Y. Cu and Co nanoparticles co-doped MIL-101 as a novel adsorbent for efficient removal of tetracycline from aqueous solutions. *Sci. Total Environ.* **2019**, *650*, 408–418. [[CrossRef](#)] [[PubMed](#)]
5. Maged, A.L.; Iqbal, J.R.; Kharbish, S.R.; Ismael, M.; Bhatnagar, A.M. Tuning tetracycline removal from aqueous solution onto activated 2:1 layered clay mineral: Characterization, sorption and mechanistic studies. *J. Hazard. Mater.* **2020**, *384*, 121320. [[CrossRef](#)] [[PubMed](#)]
6. Naderi, K.; Foroughi, M.; Azghandi, M.H.A. Tetracycline capture from aqueous solutions by nanocomposite of MWCNTs reinforced with glutaraldehyde cross-linked poly (vinyl alcohol)/chitosan. *Chemosphere* **2022**, *303*, 135124. [[CrossRef](#)] [[PubMed](#)]
7. Zhao, W.G.; Tian, Y.M.; Chu, X.X.; Cui, L.; Zhang, H.W.; Li, M.; Zhao, P. Preparation and characteristics of a magnetic carbon nanotube adsorbent: Its efficient adsorption and recoverable performances. *Sep. Purif. Technol.* **2021**, *257*, 117917. [[CrossRef](#)]
8. Chen, H.Y.; Zheng, W.F.; Zhang, F.; Li, W.X.; Shen, X.M.; Huang, H.B.; Shi, L.; Shi, R.; Zhang, S.; Lu, M. Sorption Behavior and Prediction of Tetracycline on Sediments from the Yangtze Estuary and Its Coastal Areas. *Water* **2023**, *15*, 671. [[CrossRef](#)]
9. Li, N.; Zhou, L.; Jin, X.Y.; Owens, G.; Chen, Z.L. Simultaneous removal of tetracycline and oxytetracycline antibiotics from wastewater using a ZIF-8 metal organic-framework. *J. Hazard. Mater.* **2019**, *366*, 563–572. [[CrossRef](#)]
10. Li, R.H.; Zhang, Y.C.; Deng, H.X.; Zhang, Z.Q.; Wang, J.J.; Shaheen, S.M.; Xiao, R.; Rinklebe, J.; Xi, B.D.; He, X.S.; et al. Removing tetracycline and Hg (II) with ball-milled magnetic nanobiochar and its potential on polluted irrigation water reclamation. *J. Hazard. Mater.* **2020**, *384*, 121095. [[CrossRef](#)]
11. Qiao, H.; Wang, X.X.; Liao, P.; Zhang, C.; Liu, C.X. Enhanced sequestration of tetracycline by Mn (II) encapsulated mesoporous silica nanoparticles: Synergistic sorption and mechanism. *Chemosphere* **2021**, *284*, 131334. [[CrossRef](#)] [[PubMed](#)]

12. Nguyen, V.-T.; Nguyen, T.-B.; Chen, C.-W.; Hung, C.-M.; Vo, T.-D.-H.; Chang, J.-H.; Dong, C.-D. Influence of pyrolysis temperature on polycyclic aromatic hydrocarbons production and tetracycline adsorption behavior of biochar derived from spent coffee ground. *Bioresour. Technol.* **2019**, *284*, 197–203. [[CrossRef](#)] [[PubMed](#)]
13. Kaiser, R.A.; Polk, J.S.; Datta, T.; Parekh, R.R.; Agga, G.E. Occurrence of Antibiotic Resistant Bacteria in Urban Karst Groundwater Systems. *Water* **2022**, *14*, 960. [[CrossRef](#)]
14. Sun, Y.F.; Lyu, H.H.; Cheng, Z.; Wang, Y.Z.; Tang, J.C. Insight into the mechanisms of ball-milled biochar addition on soil tetracycline degradation enhancement: Physicochemical properties and microbial community structure. *Chemosphere* **2022**, *291*, 132691. [[CrossRef](#)] [[PubMed](#)]
15. Deng, R.; Huang, D.L.; Zeng, G.M.; Wan, J.; Xue, W.J.; Wen, X.F.; Liu, X.G.; Chen, S.; Li, J.; Liu, C.H.; et al. Decontamination of lead and tetracycline from aqueous solution by a promising carbonaceous nanocomposite: Interaction and mechanisms insight. *Bioresour. Technol.* **2019**, *283*, 277–285. [[CrossRef](#)] [[PubMed](#)]
16. Huang, M.H.; Zhang, W.; Zheng, Y.; Zhang, W. Correlation among extracellular polymeric substances, tetracycline resistant bacteria and tetracycline resistance genes under trace tetracycline. *Chemosphere* **2014**, *117*, 658–662. [[CrossRef](#)]
17. Yan, L.L.; Liu, Y.; Zhang, Y.D.; Liu, S.; Wang, C.X.; Chen, W.T.; Liu, C.; Chen, Z.L.; Zhang, Y. ZnCl₂ modified biochar derived from aerobic granular sludge for developed microporosity and enhanced adsorption to tetracycline. *Bioresour. Technol.* **2020**, *297*, 122381. [[CrossRef](#)]
18. Ealias, A.M.; Saravanakumar, M.P. Facile synthesis and characterisation of AlNs using Protein Rich Solution extracted from sewage sludge and its application for ultrasonic assisted dye adsorption: Isotherms, kinetics, mechanism and RSM design. *J. Environ. Manag.* **2018**, *206*, 215–227. [[CrossRef](#)]
19. Largitte, L.; Pasquier, R. A review of the kinetics adsorption models and their application to the adsorption of lead by an activated carbon. *Chem. Eng. Res. Des.* **2016**, *109*, 495–504. [[CrossRef](#)]
20. Moon, C.; Singh, R.; Chaganti, S.R.; Lalman, J.A. Modeling sulfate removal by inhibited mesophilic mixed anaerobic communities using a statistical approach. *Water Res.* **2013**, *47*, 2341–2351. [[CrossRef](#)]
21. Chen, F.L.; Zu, Y.G.; Yang, L. A novel approach for isolation of essential oil from fresh leaves of *Magnolia sieboldii* using microwave-assisted simultaneous distillation and extraction. *Sep. Purif. Technol.* **2015**, *154*, 271–280. [[CrossRef](#)]
22. Roberson, J.A. What's Next after 40 Years of Drinking Water Regulations? *Environ. Sci. Technol.* **2011**, *45*, 154–160. [[CrossRef](#)] [[PubMed](#)]
23. Zhang, M.M.; Qiao, J.; Zhao, Z.W.; Zhang, S.F.; Qi, L. Fabrication of polymer-modified magnetic nanoparticle based adsorbents for the capture and release of quinolones by manipulating the metal-coordination interaction. *J. Sep. Sci.* **2018**, *41*, 2976–2982. [[CrossRef](#)]
24. Karri, R.R.; Sahu, J.N. Modeling and optimization by particle swarm embedded neural network for adsorption of zinc (II) by palm kernel shell based activated carbon from aqueous environment. *J. Environ. Manag.* **2018**, *206*, 178–191. [[CrossRef](#)] [[PubMed](#)]
25. Mohammad, A.T.; Abdulhameed, A.S.; Jawad, A.H. Box-Behnken design to optimize the synthesis of new crosslinked chitosan-glyoxal/TiO₂ nanocomposite: Methyl orange adsorption and mechanism studies. *Int. J. Biol. Macromol.* **2019**, *129*, 98–109. [[CrossRef](#)] [[PubMed](#)]
26. Tuzen, M.; Sari, A.; Saleh, T.A. Response surface optimization, kinetic and thermodynamic studies for effective removal of rhodamine B by magnetic AC/CeO₂ nanocomposite. *J. Environ. Manag.* **2018**, *206*, 170–177. [[CrossRef](#)]
27. Zeng, Q.; Jia, Y.W.; Xu, P.L.; Xiao, M.W.; Liu, Y.M.; Peng, S.L.; Liao, X. Quick and selective extraction of Z-ligustilide from *Angelica sinensis* using magnetic multiwalled carbon nanotubes. *J. Sep. Sci.* **2015**, *38*, 4269–4275. [[CrossRef](#)]
28. Álvarez-Uriarte, J.I.; Iriarte-Velasco, U.; Chimeno-Alanís, N.; González-Velasco, J.R. Application of Principal Component Analysis to the Adsorption of Natural Organic Matter by Modified Activated Carbons. *Sep. Sci. Technol.* **2011**, *46*, 2239–2249. [[CrossRef](#)]
29. Duan, X.H.; Liu, X.Y.; Xiao, S.H.; Du, C.; Yan, B.F. Fe-Trimesic Acid/Melamine Gel-Derived Fe/N-Doped Carbon Nanotubes as Catalyst of Peroxymonosulfate to Remove Sulfamethazine. *Water* **2023**, *15*, 381. [[CrossRef](#)]
30. Xiang, Y.J.; Xu, Z.Y.; Wei, Y.Y.; Zhou, Y.Y.; Yang, X.; Yang, Y.; Yang, J.; Zhang, J.C.; Luo, L.; Zhou, Z. Carbon-based materials as adsorbent for antibiotics removal: Mechanisms and influencing factors. *J. Environ. Manag.* **2019**, *237*, 128–138. [[CrossRef](#)]
31. Zhao, X.N.; Liu, H.Y.; Yan, Z.; Song, C. Aging of Carbon Nanotubes Increases Their Adsorption towards Tetracycline. *Water* **2022**, *14*, 2731. [[CrossRef](#)]
32. Dehghani, M.H.; Yetilmezsoy, K.; Salari, M.; Heidarinejad, Z.; Yousefi, M.; Sillanpaa, M. Adsorptive removal of cobalt (II) from aqueous solutions using multi-walled carbon nanotubes and gamma-alumina as novel adsorbents: Modelling and optimization based on response surface methodology and artificial neural network. *J. Mol. Liq.* **2020**, *299*, 112154. [[CrossRef](#)]
33. Rogelj, J.; Huppmann, D.; Krey, V.; Riahi, K.; Clarke, L.; Gidden, M.; Nicholls, Z.; Meinshausen, M. A new scenario logic for the Paris Agreement long-term temperature goal. *Nature* **2019**, *573*, 357. [[CrossRef](#)] [[PubMed](#)]
34. Mohammed, I.A.; Jawad, A.H.; Abdulhameed, A.S.; Mastuli, M.S. Physicochemical modification of chitosan with fly ash and tripolyphosphate for removal of reactive red 120 dye: Statistical optimization and mechanism study. *Int. J. Biol. Macromol.* **2020**, *161*, 503–513. [[CrossRef](#)]
35. Shahnaz, T.; Sharma, V.; Subbiah, S.; Narayanasamy, S. Multivariate optimisation of Cr (VI), Co (III) and Cu (II) adsorption onto nanobentonite incorporated nanocellulose/chitosan aerogel using response surface methodology. *J. Water Process. Eng.* **2020**, *36*, 12. [[CrossRef](#)]

36. Bonetto, L.R.; Crespo, J.S.; Guegan, R.; Esteves, V.I.; Giovanela, M. Removal of methylene blue from aqueous solutions using a solid residue of the apple juice industry: Full factorial design, equilibrium, thermodynamics and kinetics aspects. *J. Mol. Struct.* **2021**, *1224*, 14. [[CrossRef](#)]
37. Dil, E.A.; Doustimotlagh, A.H.; Javadian, H.; Asfaram, A.; Ghaedi, M. Nano-sized Fe₃O₄@SiO₂-molecular imprinted polymer as a sorbent for dispersive solid-phase microextraction of melatonin in the methanolic extract of *Portulaca oleracea*, biological, and water samples. *Talanta* **2021**, *221*, 10. [[CrossRef](#)]
38. Rasoulzadeh, H.; Dehghani, M.H.; Mohammadi, A.S.; Karri, R.R.; Nabizadeh, R.; Nazmara, S.; Kim, K.H.; Sahu, J.N. Parametric modelling of Pb (II) adsorption onto chitosan-coated Fe₃O₄ particles through RSM and DE hybrid evolutionary optimization framework. *J. Mol. Liq.* **2020**, *297*, 111893. [[CrossRef](#)]
39. Madrakian, T.; Afkhami, A.; Ahmadi, M.; Bagheri, H. Removal of some cationic dyes from aqueous solutions using magnetic-modified multi-walled carbon nanotubes. *J. Hazard. Mater.* **2011**, *196*, 109–114. [[CrossRef](#)]
40. Azad, F.N.; Ghaedi, M.; Dashtian, K.; Hajati, S.; Pezeshkpour, V. Ultrasonically assisted hydrothermal synthesis of activated carbon-HKUST-1-MOF hybrid for efficient simultaneous ultrasound-assisted removal of ternary organic dyes and antibacterial investigation: Taguchi optimization. *Ultrason. Sonochem.* **2016**, *31*, 383–393. [[CrossRef](#)]
41. Gadekar, M.R.; Ahammed, M.M. Modelling dye removal by adsorption onto water treatment residuals using combined response surface methodology-artificial neural network approach. *J. Environ. Manag.* **2019**, *231*, 241–248. [[CrossRef](#)] [[PubMed](#)]
42. Yu, R.F.; Lin, C.H.; Chen, H.W.; Cheng, W.P.; Kao, M.C. Possible control approaches of the Electro-Fenton process for textile wastewater treatment using on-line monitoring of DO and ORP. *Chem. Eng. J.* **2013**, *218*, 341–349. [[CrossRef](#)]
43. Turan, N.G.; Mesci, B.; Ozgonenel, O. The use of artificial neural networks (ANN) for modeling of adsorption of Cu(II) from industrial leachate by pumice. *Chem. Eng. J.* **2011**, *171*, 1091–1097. [[CrossRef](#)]
44. Dolatabadi, M.; Mehrabpour, M.; Esfandyari, M.; Alidadi, H.; Davoudi, M. Modeling of simultaneous adsorption of dye and metal ion by sawdust from aqueous solution using of ANN and ANFIS. *Chemometrics Intell. Lab. Syst.* **2018**, *181*, 72–78. [[CrossRef](#)]
45. Sen Gupta, S.; Bhattacharyya, K.G. Kinetics of adsorption of metal ions on inorganic materials: A review. *Adv. Colloid Interface Sci.* **2011**, *162*, 39–58. [[CrossRef](#)]
46. Karri, R.R.; Tanzifi, M.; Yarak, M.T.; Sahu, J.N. Optimization and modeling of methyl orange adsorption onto polyaniline nano-adsorbent through response surface methodology and differential evolution embedded neural network. *J. Environ. Manag.* **2018**, *223*, 517–529. [[CrossRef](#)]
47. Karthikeyan, S.; Gupta, V.K.; Boopathy, R.; Titus, A.; Sekaran, G. A new approach for the degradation of high concentration of aromatic amine by heterocatalytic Fenton oxidation: Kinetic and spectroscopic studies. *J. Mol. Liq.* **2012**, *173*, 153–163. [[CrossRef](#)]
48. Sun, Y.R.; Yang, Y.X.; Yang, M.X.; Yu, F.; Ma, J. Response surface methodological evaluation and optimization for adsorption removal of ciprofloxacin onto graphene hydrogel. *J. Mol. Liq.* **2019**, *284*, 124–130. [[CrossRef](#)]
49. Mutalik, S.P.; Mullick, P.; Pandey, A.; Kulkarni, S.S.; Mutalik, S. Box-Behnken design aided optimization and validation of developed reverse phase HPLC analytical method for simultaneous quantification of dolutegravir sodium and lamivudine co-loaded in nano-liposomes. *J. Sep. Sci.* **2021**, *44*, 2917–2931. [[CrossRef](#)]
50. Shah, K.J.; Yu, J.C.; Zhang, T.; You, Z.Y. Y-Type Zeolite Synthesized from an Illite Applied for Removal of Pb(II) and Cu(II) Ions from Aqueous Solution: Box-Behnken Design and Kinetics. *Water* **2023**, *15*, 1171. [[CrossRef](#)]
51. Dalvand, A.; Nabizadeh, R.; Ganjali, M.R.; Khoobi, M.; Nazmara, S.; Mahvi, A.H. Modeling of Reactive Blue 19 azo dye removal from colored textile wastewater using L-arginine-functionalized Fe₃O₄ nanoparticles: Optimization, reusability, kinetic and equilibrium studies. *J. Magn. Magn. Mater.* **2016**, *404*, 179–189. [[CrossRef](#)]
52. Murugesan, A.; Vidhyadevi, T.; Kalaivani, S.S.; Thiruvengadaravi, K.V.; Ravikumar, L.; Anuradha, C.D.; Sivanesan, S. Modelling of lead (II) ion adsorption onto poly (thiourea imine) functionalized chelating resin using response surface methodology (RSM). *J. Water Process. Eng.* **2014**, *3*, 132–143. [[CrossRef](#)]
53. Yang, Y.Q.; Zheng, Z.H.; Zhang, D.F.; Zhang, X.D. Response surface methodology directed adsorption of chlorate and chlorite onto MIEX resin and study of chemical properties. *Environ. Sci.-Wat. Res. Technol.* **2020**, *6*, 2454–2464. [[CrossRef](#)]
54. Demircivi, P.; Bugdayci, M. Synthesis and thermodynamic simulation of Zr Doped SrAl₂O₄ ceramic powders: Enhanced adsorptive properties for antibiotic tetracycline. *Mater. Res. Express.* **2019**, *6*, 12. [[CrossRef](#)]
55. Haghghat, G.A.; Saghi, M.H.; Anastopoulos, I.; Javid, A.; Roudbari, A.; Talebi, S.S.; Ghadiri, S.K.; Giannakoudakis, D.A.; Shams, M. Aminated graphitic carbon derived from corn stover biomass as adsorbent against antibiotic tetracycline: Optimizing the physicochemical parameters. *J. Mol. Liq.* **2020**, *313*, 9. [[CrossRef](#)]
56. El Messaoudi, N.; El Khomri, M.; Ablouh, E.H.; Bouich, A.; Lacherai, A.; Jada, A.; Lima, E.C.; Sher, F. Biosynthesis of SiO₂ nanoparticles using extract of *Nerium oleander* leaves for the removal of tetracycline antibiotic. *Chemosphere* **2022**, *287*, 10. [[CrossRef](#)]
57. Gu, S.Y.; Zhang, D.F.; Gao, Y.Q.; Qi, R.Z.; Chen, W.F.; Xu, Z.H. Fabrication of porous carbon derived from cotton/polyester waste mixed with oyster shells: Pore-forming process and application for tetracycline removal. *Chemosphere* **2021**, *270*, 12. [[CrossRef](#)]
58. Ashrafi, S.D.; Safari, G.H.; Sharafi, K.; Kamani, H.; Jaafari, J. Adsorption of 4-Nitrophenol on calcium alginate-multiwall carbon nanotube beads: Modeling, kinetics, equilibriums and reusability studies. *Int. J. Biol. Macromol.* **2021**, *185*, 66–76. [[CrossRef](#)]
59. Islam, A.; Chauhan, A.; Javed, H.; Rais, S.; Ahmad, I. Magnetic Carbon Nanotubes-Silica Binary Composite for Effective Pb(II) Sequestration from Industrial Effluents: Multivariate Process Optimization. *Clean-Soil Air Water* **2021**, *49*, 10. [[CrossRef](#)]

60. Huacalco-Aguilar, Y.; Alvarez-Torrellas, S.; Martinez-Nieves, J.; Delgado-Adamez, J.; Gil, M.V.; Ovejero, G.; Garcia, J. Magnetite-Based Catalyst in the Catalytic Wet Peroxide Oxidation for Different Aqueous Matrices Spiked with Naproxen-Diclofenac Mixture. *Catalysts* **2021**, *11*, 514. [[CrossRef](#)]
61. Aliyu, A. Synthesis, electron microscopy properties and adsorption studies of Zinc (II) ions (Zn^{2+}) onto as-prepared Carbon Nanotubes (CNTs) using Box-Behnken Design (BBD). *Sci. Afr.* **2019**, *3*, e00069. [[CrossRef](#)]
62. Thiyagarajan, P.; Selvam, K.; Sudhakar, C.; Selvankumar, T. Enhancement of Adsorption of Magenta Dye by Immobilized Laccase on Functionalized Biosynthesized Activated Carbon Nanotubes. *Water Air Soil Pollut.* **2020**, *231*, 364. [[CrossRef](#)]
63. Osaghi, B.; Safa, F. Cloud Point Extraction in Presence of Multi-walled Carbon Nanotubes for Removal of Direct Green 26 from Aqueous Solutions: Optimization by Box-Behnken Design and Desirability Functions. *J. Anal. Chem.* **2020**, *75*, 802–811. [[CrossRef](#)]
64. Tomaszewska, J.; Smektala, P.; Zglobicka, I.; Michalski, J.; Kurzydowski, K.J.; Krzeminski, P. Escudero-Onate, C. Non-woven polypropylene fabric modified with carbon nanotubes and decorated with nanoakaganeite for arsenite removal. *Int. J. Environ. Sci. Technol.* **2018**, *15*, 1831–1842. [[CrossRef](#)]
65. Safa, F.; Osaghi, B. Adsorption onto MWCNTs Coupled with Cloud Point Extraction for Dye Removal from Aqueous Solutions: Optimization by Experimental Design. *Comb. Chem. High Throughput Screen.* **2021**, *24*, 246–258. [[CrossRef](#)]
66. Tayeb, A.M.; Hussein, D.S.; Farouq, R. Optimization of photocatalytic degradation of methylene blue dye using titanate nanotube. *J. Nanophotonics* **2020**, *14*, 026008. [[CrossRef](#)]
67. Cao, J.Y.; Xiong, Z.K.; Lai, B. Effect of initial pH on the tetracycline (TC) removal by zero-valent iron: Adsorption, oxidation and reduction. *Chem. Eng. J.* **2018**, *343*, 492–499. [[CrossRef](#)]
68. Gao, Y.; Li, Y.; Zhang, L.; Huang, H.; Hu, J.J.; Shah, S.M.; Su, X.G. Adsorption and removal of tetracycline antibiotics from aqueous solution by graphene oxide. *J. Colloid Interface Sci.* **2012**, *368*, 540–546. [[CrossRef](#)]
69. Liu, P.; Liu, W.-J.; Jiang, H.; Chen, J.-J.; Li, W.-W.; Yu, H.-Q. Modification of bio-char derived from fast pyrolysis of biomass and its application in removal of tetracycline from aqueous solution. *Bioresour. Technol.* **2012**, *121*, 235–240. [[CrossRef](#)]
70. Zeng, Z.T.; Ye, S.J.; Wu, H.P.; Xiao, R.; Zeng, G.M.; Liang, J.; Zhang, C.; Yu, J.F.; Fang, Y.L.; Song, B. Research on the sustainable efficacy of g-MoS₂ decorated biochar nanocomposites for removing tetracycline hydrochloride from antibiotic-polluted aqueous solution. *Sci. Total Environ.* **2019**, *648*, 206–217. [[CrossRef](#)]
71. Jun, L.Y.; Karri, R.R.; Yon, L.S.; Mubarak, N.M.; Bing, C.H.; Mohammad, K.; Jagadish, P.; Abdullah, E.C. Modeling and optimization by particle swarm embedded neural network for adsorption of methylene blue by jicama peroxidase immobilized on buckypaper/polyvinyl alcohol membrane. *Environ. Res.* **2020**, *183*, 109158. [[CrossRef](#)]
72. Karimifard, S.; Moghaddam, M.R.A. Corrigendum to “Application of response surface methodology in physicochemical removal of dyes from wastewater: A critical review” (*Sci. Total Environ.* 2018, 640, 772). *Sci. Total Environ.* **2019**, *650*, 696. [[CrossRef](#)]
73. Khodaie, M.; Ghasemi, N.; Moradi, B.; Rahimi, M. Removal of Methylene Blue from Wastewater by Adsorption onto ZnCl₂ Activated Corn Husk Carbon Equilibrium Studies. *J. Chem.* **2013**, *2013*, 383985. [[CrossRef](#)]
74. Oladoja, N.A.; Akinlabi, A.K. Congo Red Biosorption on Palm Kernel Seed Coat. *Ind. Eng. Chem. Res.* **2009**, *48*, 6188–6196. [[CrossRef](#)]
75. Huang, B.Y.; Liu, Y.G.; Li, B.; Liu, S.B.; Zeng, G.M.; Zeng, Z.W.; Wang, X.H.; Ning, Q.M.; Zheng, B.H.; Yang, C.P. Effect of Cu (II) ions on the enhancement of tetracycline adsorption by Fe₃O₄@SiO₂-Chitosan/graphene oxide nanocomposite. *Carbohydr. Polym.* **2017**, *157*, 576–585. [[CrossRef](#)] [[PubMed](#)]
76. Zhang, P.Z.; Li, Y.F.; Cao, Y.Y.; Han, L.J. Characteristics of tetracycline adsorption by cow manure biochar prepared at different pyrolysis temperatures. *Bioresour. Technol.* **2019**, *285*, 121348. [[CrossRef](#)] [[PubMed](#)]
77. Ho, Y.-S.; McKay, G. Pseudo-second order model for sorption processes. *Process Biochem.* **1999**, *34*, 451–465. [[CrossRef](#)]
78. Yue, Y.M.; Zhang, P.X.; Wang, W.; Cai, Y.C.; Tan, F.T.; Wang, X.Y.; Qiao, X.L.; Wong, P.K. Enhanced dark adsorption and visible-light-driven photocatalytic properties of narrower-band-gap Cu₂S decorated Cu₂O nanocomposites for efficient removal of organic pollutants. *J. Hazard. Mater.* **2020**, *384*, 121302. [[CrossRef](#)]
79. Zhang, X.Y.; Gu, P.; Li, X.Y.; Zhang, G.H. Efficient adsorption of radioactive iodide ion from simulated wastewater by nano Cu₂O/Cu modified activated carbon. *Chem. Eng. J.* **2017**, *322*, 129–139. [[CrossRef](#)]
80. Jing, X.-R.; Wang, Y.-Y.; Liu, W.-J.; Wang, Y.-K.; Jiang, H. Enhanced adsorption performance of tetracycline in aqueous solutions by methanol-modified biochar. *Chem. Eng. J.* **2014**, *248*, 168–174. [[CrossRef](#)]
81. Zhou, Y.Y.; Liu, X.C.; Xiang, Y.J.; Wang, P.; Zhang, J.C.; Zhang, F.F.; Wei, J.H.; Luo, L.; Lei, M.; Tang, L. Modification of biochar derived from sawdust and its application in removal of tetracycline and copper from aqueous solution: Adsorption mechanism and modelling. *Bioresour. Technol.* **2017**, *245*, 266–273. [[CrossRef](#)] [[PubMed](#)]
82. Chao, Y.H.; Zhu, W.S.; Wu, X.Y.; Hou, F.F.; Xun, S.H.; Wu, P.W.; Ji, H.Y.; Xu, H.; Li, H.M. Application of graphene-like layered molybdenum disulfide and its excellent adsorption behavior for doxycycline antibiotic. *Chem. Eng. J.* **2014**, *243*, 60–67. [[CrossRef](#)]
83. Ji, L.L.; Chen, W.; Duan, L.; Zhu, D.Q. Mechanisms for strong adsorption of tetracycline to carbon nanotubes: A comparative study using activated carbon and graphite as adsorbents. *Environ. Sci. Technol.* **2009**, *43*, 2322–2327. [[CrossRef](#)] [[PubMed](#)]
84. Zbair, M.; Anfar, Z.; Ahsaine, H.A.; El Alem, N.; Ezahri, M. Acridine orange adsorption by zinc oxide/almond shell activated carbon composite: Operational factors, mechanism and performance optimization using central composite design and surface modeling. *J. Environ. Manag.* **2018**, *206*, 383–397. [[CrossRef](#)]
85. Peiris, C.; Gunatilake, S.R.; Mlsna, T.E.; Mohan, D.; Vithanage, M. Biochar based removal of antibiotic sulfonamides and tetracyclines in aquatic environments: A critical review. *Bioresour. Technol.* **2017**, *246*, 150–159. [[CrossRef](#)]

86. Zhou, Y.; Zhang, L.; Cheng, Z.J. Removal of organic pollutants from aqueous solution using agricultural wastes: A review. *J. Mol. Liq.* **2015**, *212*, 739–762. [[CrossRef](#)]
87. Danmaliki, G.I.; Saleh, T.A.; Shamsuddeen, A.A. Response surface methodology optimization of adsorptive desulfurization on nickel/activated carbon. *Chem. Eng. J.* **2017**, *313*, 993–1003. [[CrossRef](#)]
88. Zhao, W.X.; Ma, A.Q.; Ji, J.H.; Chen, X.; Yao, T. Multiobjective Optimization of a Double-Side Linear Vernier PM Motor Using Response Surface Method and Differential Evolution. *IEEE Trans. Ind. Electron.* **2020**, *67*, 80–90. [[CrossRef](#)]
89. Kafshgari, L.A.; Ghorbani, M.; Azizi, A.; Agarwal, S.; Gupta, V.K. Modeling and optimization of Direct Red 16 adsorption from aqueous solutions using nanocomposite of MnFe₂O₄/MWCNTs: RSM-CCRD model. *J. Mol. Liq.* **2017**, *233*, 370–377. [[CrossRef](#)]
90. Asfaram, A.; Ghaedi, M.; Hajati, S.; Goudarzi, A.; Dil, E.A. Screening and optimization of highly effective ultrasound-assisted simultaneous adsorption of cationic dyes onto Mn-doped Fe₃O₄-nanoparticle-loaded activated carbon. *Ultrason. Sonochem.* **2017**, *34*, 1–12. [[CrossRef](#)]
91. Ranch, K.M.; Maulvi, F.A.; Naik, M.J.; Koli, A.R.; Parikh, R.K.; Shah, D.O. Optimization of a novel in situ gel for sustained ocular drug delivery using Box-Behnken design: In vitro, ex vivo, in vivo and human studies. *Int. J. Pharm.* **2019**, *554*, 264–275. [[CrossRef](#)] [[PubMed](#)]

Disclaimer/Publisher’s Note: The statements, opinions and data contained in all publications are solely those of the individual author(s) and contributor(s) and not of MDPI and/or the editor(s). MDPI and/or the editor(s) disclaim responsibility for any injury to people or property resulting from any ideas, methods, instructions or products referred to in the content.